*Issued as NRC No. 11765.
[1]M. J. P. Musgrave, Proc. Roy. Soc. (London) 226, 346 (1954).
[2]J. Bardeen and D. Pines, Phys. Rev. 99, 1140 (1955).
[3]E. Y. Wang, R. J. Kolouch, and K. A. McCarthy, Phys. Rev. 175, 723 (1968).
[4]O. P. Katyal and A. N. Gerritsen, Phys. Rev. 185, 1017 (1969).
[5]A. Mooradian and G. B. Wright, Phys. Rev. Letters 16, 999 (1966).
[6]K. S. Singwi and M. P. Tosi, Phys. Rev. 147, 658 (1966).
[7]E-Ni. Foo and N. Tzoar, Phys. Rev. 185, 644 (1969).

PHYSICAL REVIEW B VOLUME 3, NUMBER 10 15 MAY 1971

Anomalous Behavior of the Cyclotron Resonance of Holes in Bismuth

Jun'ichirō Nakahara, Hajimu Kawamura, and Yasuji Sawada
Department of Physics, Osaka University, Toyonaka, Japan
(Received 16 September 1970)

The cyclotron resonance of holes in bismuth has been carefully investigated using microwaves of frequency 50 GHz in the Azbel'-Kaner configuration. It was found that the reflection peak is extremely weak at the fundamental but strong at the second harmonic, and the second-harmonic line shape may be quite complicated. These anomalous effects may be explained if the longitudinal magnetoplasma excitations in the vicinity of the second harmonic (Bernstein mode) are coupled with the electromagnetic waves of a magnetoplasma (Alfvén waves) in the weakly nonlocal regime. As a result, the location of the reflection peaks shifts from that of the exact cyclotron harmonics. Taking into account these shifts, we determined the cyclotron masses of holes to be $(0.210 \pm 0.002)m_0$ for $\vec{B} \perp \vec{E}_{rf}$ and $(0.217 \pm 0.002)m_0$ for $\vec{B} \parallel \vec{E}_{rf}$.

I. INTRODUCTION

A considerable number of experimental and theoretical investigations[1–6] have been performed on magnetoplasmas in bismuth in the microwave frequency region for the Voigt configuration.

The magnetoplasmas in bismuth have been investigated through the tilted-orbit cyclotron resonances,[2] hybrid resonances,[2] Alfvén waves,[7–11] and Azbel'-Kaner cyclotron resonances.[3,4,12] While the first three of these are observed for the classical skin effect condition, the last is observed in the extremely anomalous condition. However, in practice the hole cyclotron resonances in bismuth occur in a weakly nonlocal condition, especially in the case that the hole cyclotron frequency is less than the electron-hole hybrid resonance frequency.

Hebel[6] has discussed a slightly anomalous skin effect for the rf electric fields of the microwaves parallel to the static magnetic field ($\vec{E}_{rf} \parallel \vec{B}$; ordinary configuration). He found that the cyclotron resonance due to the dipole transition arising from the transverse excitation occurs only for the fundamental in this case. However, in the extraordinary configuration the longitudinal component of the dielectric constants should play an important role.

In this paper we shall present both the experimental results and the theoretical calculations for the anomalous line shape of hole cyclotron resonances in bismuth, especially for the extraordinary configuration. Our data indicate that the reflection peak near the second harmonic is stronger than the peak associated with either the fundamental or other harmonics. In addition, the line shape of the reflection peak may be quite complicated. This behavior is quite different from those for metals with large values of $\omega\tau$, in which case the line shapes depend upon the structure of the Fermi surface as was explained by Chambers[13] and experimentally shown by Moore.[14]

II. PLASMA EXCITATION AND PHOTON-PLASMA COUPLED MODE

The Azbel'-Kaner cyclotron resonances for metals have been discussed in terms of surface impedance.[15–17] In Sec. IV we shall analyze the line shapes of the microwave reflection from this viewpoint and compare with experimental results. In this section we shall present a preliminary discussion using the dispersion relations for plasma excitations. We shall assume for simplicity that the energy surfaces are spherical.

Throughout our treatment we assume that the static magnetic field $\vec{B}$ is oriented along the z axis, and the wave vector $\vec{q}$ is parallel to the x axis of a Cartesian coordinate system. The dispersion relations for magnetoplasma excitations as well as the coupled modes of excitations between electromagnetic waves and plasma can be given in terms of the dielectric functions

$$\overleftrightarrow{\epsilon} = \begin{pmatrix} \epsilon_{xx} & \epsilon_{xy} & 0 \\ \epsilon_{yx} & \epsilon_{yy} & 0 \\ 0 & 0 & \epsilon_{zz} \end{pmatrix} . \tag{1}$$

When the carriers are degenerate and Landau-level spacings are much less than the Fermi energy ($E_F \gg kT, \hbar\omega_c$), the components of this tensor are given by[18]

$$\epsilon_{xx} = \frac{3\epsilon'}{X^2} \sum_{n=-\infty}^{+\infty} \frac{n^2 g_n(X)}{1 + i(n\omega_c - \omega)\tau} + \epsilon_l , \tag{2a}$$

$$\epsilon_{yy} = 3\epsilon' \sum_{n=-\infty}^{+\infty} \frac{s_n(X)}{1 + i(n\omega_c - \omega)\tau} + \epsilon_l , \tag{2b}$$

$$\epsilon_{xy} = -\epsilon_{yx} = \frac{3\epsilon'}{2X} \sum_{n=-\infty}^{+\infty} \frac{in g_n'(X)}{1 + i(n\omega_c - \omega)\tau} , \tag{2c}$$

and

$$\epsilon_{zz} = 3\epsilon' \sum_{n=-\infty}^{+\infty} \frac{r_n(X)}{1 + i(n\omega_c - \omega)\tau} + \epsilon_l , \tag{2d}$$

where

$$g_n(X) = \sum_{m=0}^{\infty} (-1)^m \frac{X^{2m+2n}}{m!(m+2n)!(2m+2n+1)} , \tag{3a}$$

$$s_n(X) = \left(2 + \frac{n^2}{X^2}\right) g_n(X) - 3 \sum_{m=0}^{\infty} \frac{(-1)^m (2m+2n+2) X^{2m+2n}}{m!(m+2n)!(2m+2n+1)(2m+2n+3)} , \tag{3b}$$

$$r_n(X) = \sum_{m=0}^{\infty} \frac{(-1)^m X^{2m+2n}}{m!(m+2n)!(2m+2n+1)(2m+2n+3)} , \tag{3c}$$

and

$$\epsilon' = \frac{4\pi}{i\omega} \frac{Ne^2\tau}{m^*} , \qquad X = qR. \tag{3d}$$

The symbols N, m^*, ω_c, R, and τ are the density, effective mass, cyclotron frequency, cyclotron radius, and relaxation time of the carriers, respectively.

The longitudinal excitation occurs when the condition

$$\epsilon_{xx} = 0 \tag{4}$$

is fulfilled. The conditions for transverse excitations are given by the following equations:

$$\epsilon_{yy} = \infty \tag{5}$$

or

$$\epsilon_{zz} = \infty . \tag{6}$$

From these relations we can determine the dispersion relations for those excitations if the frequency and the wave-number-dependent dielectric functions shown in (2) are employed. Electromagnetic waves couple with these magnetoplasma excitations. One of these coupled modes is polarized along the magnetic field (ordinary mode) and the other mode is polarized in the plane normal to the magnetic field (extraordinary mode). The dispersion relations of these coupled modes can be obtained from the Maxwell's equations with q-dependent dielectric functions. The results are given by

$$[(c/\omega)q]^2 = \epsilon_{zz} \tag{7}$$

for the ordinary mode, and

$$[(c/\omega)q]^2 = (\epsilon_{yy}\epsilon_{xx} + \epsilon_{xy}^2)/\epsilon_{xx} \tag{8}$$

for the extraordinary mode. These coupled modes do not penetrate into metals in the local regime,[19] and the skin depth is usually much smaller than the cyclotron radius. In this case, $\epsilon_{xx}\epsilon_{yy}$ is larger than ϵ_{xy}^2 by the order of qR, and ϵ_{yy} is approximately equal to ϵ_{zz}. Then Eqs. (7) and (8) become identical and are written as

$$[(c/\omega)q]^2 = \epsilon_{zz} \approx \epsilon_{yy} .$$

Anomalies of this mode occur only at the poles of ϵ_{zz}, i.e, $\omega = n\omega_c$. This is the well-known Azbel'-Kaner cyclotron resonance, which is therefore a pure transverse excitation. On the other hand, the extraordinary mode (8) can penetrate into semimetals in the local regime when the field strength is greater than that at which hybrid resonance occurs. This is the so-called Alfvén wave in Voigt configuration. In this case qR is usually smaller than unity in the neighborhood of the lower harmonic cyclotron excitations for the heavier mass carriers. These excitations are located in the transparent region. Then the oscillator strengths $g_n(X)$, $s_n(X)$, and $r_n(X)$ can be expanded as a power series of $(qR)^2$ as shown in (3a)–(3c). From these equations, we find that $\epsilon_{xx}\epsilon_{yy}$ is of the same order of magnitude as ϵ_{xy}^2, so that the singular points of q in the left-hand side of the Eq. (8) are approximately given by $\epsilon_{xx} = 0$, which is the condition for longitudinal excitations. As a result of the coupling with these longitudinal excitations, an anomalous reflection of electromagnetic waves is expected near the cyclotron harmonics.

We have solved Eq. (8) for a fictitious semimetal having spherical electron and hole energy surfaces. The dielectric functions were expanded up to X^{20} and the roots were found graphically. The model chosen to simulate bismuth with the magnetic field parallel to the bisectrix axis has the following features: (a) electron mass $= 0.02 m_0$, hole mass $= 0.21 m_0$; and (b) carrier densities for electrons and holes $= 2.9 \times 10^{17}$ cm^{-3}. In Fig. 1 the re-

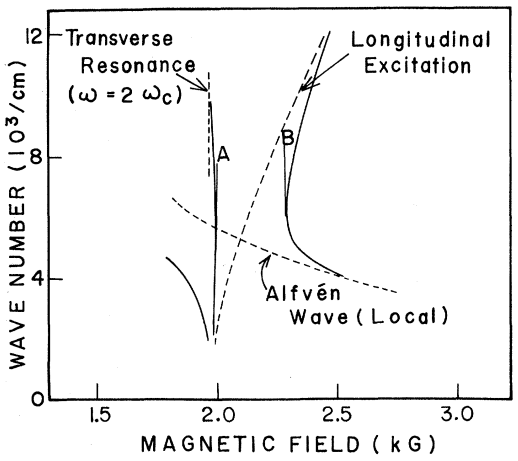

FIG. 1. Wave number for the extraordinary mode as a function of magnetic field near the second-harmonic cyclotron resonance. $\omega = 2\omega_c$. The spherical energy surface model is chosen to simulate bismuth with the magnetic field parallel to the bisectrix axis.

sults of the calculation in the neighborhood of the second harmonic of the hole cyclotron field are shown as solid lines. The microwave frequency is assumed to be 52.5 GHz, and the effect of carrier scattering is neglected. In Fig. 1 the longitudinal excitation, transverse excitation, and the local Alfvên wave mode are shown as dashed lines. The solid line indicates the coupling of the Alfvên waves with longitudinal or transverse excitation. Strong microwave reflection would be expected to occur between points A and B, since in this region the real wave number does not exist as a consequence of the assumption of an infinite relaxation time. Later we shall show that for the weakly nonlocal plasma ($qR \ll 1$) such a strong reflection peak is not expected to occur for either the fundamental or the third and higher harmonics, and the anomaly in the dispersion relation near the fundamental is negligibly small.

The transverse excitation ($\epsilon_{yy} = \infty$) occurs at each cyclotron harmonic with the dispersion relation indicated by vertical line as in Fig. 1. However, all the transverse excitations disappear at the lowest-order expansion (X^2), since the longitudinal electric field creates a space charge which shields out the transverse resonances in the lowest order.[20] If we include the next higher-order terms (X^4), the transverse excitations at the fundamental and the second harmonic appear.

The longitudinal excitation near the harmonics of hole cyclotron resonance in the approximation including up to terms X^2 can be obtained from the following equation:

$$\epsilon_{xx} = \epsilon_0 + \frac{\omega_{p1}^2}{\omega_c^2 - \omega^2} + \frac{\omega_{p2}^2}{(2\omega_c)^2 - \omega^2} = 0 \quad , \tag{9}$$

where the oscillator strengths ω_{p1}^2 and ω_{p2}^2 are given by

$$\omega_{p1}^2 = \omega_p^2 (1 - \tfrac{1}{5} X^2) \quad \text{and} \quad \omega_{p2}^2 = \tfrac{1}{5} \omega_p^2 X^2 \quad . \tag{10}$$

In the region of the hole cyclotron harmonics the electrons contribute to the dielectric functions with a term nearly independent of cyclotron frequency, so that the constant term ϵ_0 of Eq. (9) includes the effect from electrons. The solutions of Eq. (8) for $\omega_p^2/\epsilon_0 \gg \omega_c^2$ are given by

$$\omega_+^2 = \omega_p^2/\epsilon_0 + \omega_c^2 + \tfrac{3}{5} \omega_c^2 X^2 \quad , \tag{11}$$

$$\omega_-^2 = (2\omega_c)^2 - \tfrac{3}{5} \omega_c^2 X^2 \quad . \tag{12}$$

The higher mode (ω_+) is the well-known magnetoplasma excitation which exists even for $q = 0$. The lower mode (ω_-), which can exist only for finite q, corresponds to the Bernstein mode[21,22] in a nondegenerate plasma. This excitation (ω_-) appears only in the vicinity of the second harmonic in a long-wavelength approximation up to the order of X^2. It is interesting to note that for this mode the group velocity and the phase velocity are in opposite directions. It is also interesting that the longitudinal excitation appears only in the vicinity of the second harmonic and the hybrid plasma mode. If the next higher-order terms up to X^4 are included, the longitudinal excitations at the third harmonic appear. The longitudinal excitations near the nth harmonic appear at X^{2n-2}, but the transverse excitations appear at X^{2n}. Therefore, the longitudinal excitation near the second harmonic is exceptionally strong at the weakly nonlocal limit.

For the ordinary mode, the fundamental cyclotron resonance has been explained by Hebel[6] on the basis of the surface nonlocal effect for a long-wavelength approximation of the lowest order. These resonances can be explained considering just the bulk properties and will appear in the dielectric function expansion if higher-order terms are kept. In both treatments only the transverse resonances occur. The oscillator strength for cyclotron harmonics are $X^2/30$ for the fundamental and $X^4/840$ for the second harmonic when X is less than unity. Thus the fundamental cyclotron resonance is much stronger than the second harmonic in contrast to the extraordinary case.

III. EXPERIMENTAL

For the present experiments, bismuth single crystals of ultrahigh purity were used with $\omega\tau$ more than 100 resulting in sharply defined spectra. Commercially available bismuth metals of nominal purity of 99.9999% were zone refined 30 times in a high vacuum of better than 7×10^{-7} mm Hg, and crystallized in a high-purity carbon boat. The specimens were machined to the desired shape using a spark

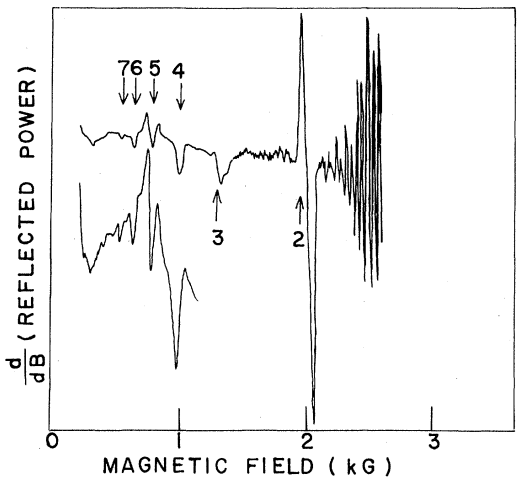

FIG. 2. Microwave reflection from a slab of a bismuth single crystal as a function of magnetic field (derivative curve). In this figure $\vec{q} \parallel$ binary, $\vec{B} \parallel$ bisectrix, $\vec{E}_{rf} \parallel$ trigonal axis; $f = 52.5$ GHz; $T = 1.6$ °K. The sample thickness d is 0.715 ± 0.003 mm.

cutter and spark planer. The surface layers were removed with 30% nitric acid, and the surface was electropolished until it became optically flat.

The experiments have been carried out using standard microwave techniques at frequencies near 50 GHz with magnetic field modulation at 95 Hz and phase-sensitive detection techniques. The sample was mounted on a choke joint in a horizontal plane forming one end wall of a TE_{113} cylindrical cavity. This cavity had two orthogonal degenerate modes in which the microwave currents across the wall are perpendicular to each other. In our cavity, one mode is about ten times stronger than the other, as was checked by the electron-spin-resonance (ESR) signal of DPPH. The experimentally obtained signals are proportional to the field derivative of reflected power from the surface of the specimen, which is proportional to the derivative of the real part of the surface impedance Z when $\frac{1}{4}c \gg Z$. All data were taken at 1.6 °K, where the linewidths were about $\frac{3}{4}$ as narrow as those at 4.2 °K.

Figures 2–5 show the field derivative of the reflected power for various configurations. Figure 2 is obtained from a specimen of thickness 0.715 mm with parallel planes in the configuration that $\vec{q}$ is along a binary axis, $\vec{B}$ along the bisectrix axis, and $\vec{E}_{rf}$ along the trigonal axis. The Fabry-Perot interference pattern from the Alfvén waves and the "Azbel'-Kaner cyclotron resonance" at second and higher harmonics of the holes are observed. The fundamental resonance is so weak that is is masked by the interference pattern of dimensional resonances. These interference patterns can be solved to obtain the wave number q of the Alfvén waves, using the condition $qd = \pi N$, where d is the thickness of the specimen and N is the fringe number. The wave number q obtained in this manner is plotted in Fig. 3 as a function of magnetic field B for the configuration $\vec{q} \parallel$ binary, $\vec{B} \parallel$ bisectrix, and $\vec{E}_{rf} \parallel$ trigonal axis. The experimental points are in excellent agreement with the solid line obtained by solving the dispersion relation in Eq. (8) for nonlocal q-dependent anisotropic dielectric functions for bismuth.[23] We have neglected the off-diagonal elements of the dielectric tensor for electrons arising from the tilting of the electron energy surfaces, since they have very little effect on our results. The dispersion relations for the longitudinal mode ω_- and Alfvén waves in the local limit are shown in this figure as dashed lines. The calculation was based on Eq. (12). Near the second harmonic, the wavelength of the Alfvén waves is about 15 times as large as the cyclotron radius. As was discussed in Sec. II, the singularity near the second harmonic is interpreted as the coupling of longitudinal excita-

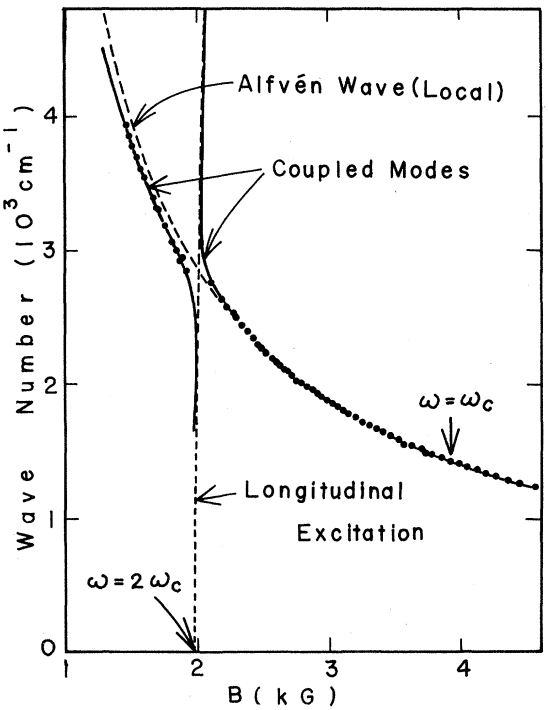

FIG. 3. Dispersion relation for electromagnetic waves for $f = 52.5$ GHz in the vicinity of the second harmonic ($1970g$) and the fundamental ($3940g$) of the hole cyclotron resonances. The solid lines are the calculated curves for the electromagnetic waves coupled with longitudinal excitations (nonlocal Alfvén waves), and the dashed lines are the calculated curves for Alfvén waves in the local regime and the longitudinal excitation ω_- (nonlocal). In the coupled wave calculation $\omega\tau$ is assumed to be 100; in both the local Alfvén wave and the longitudinal excitation cases, $\omega\tau = \infty$. Dots are the experimental points obtained from interference patterns.

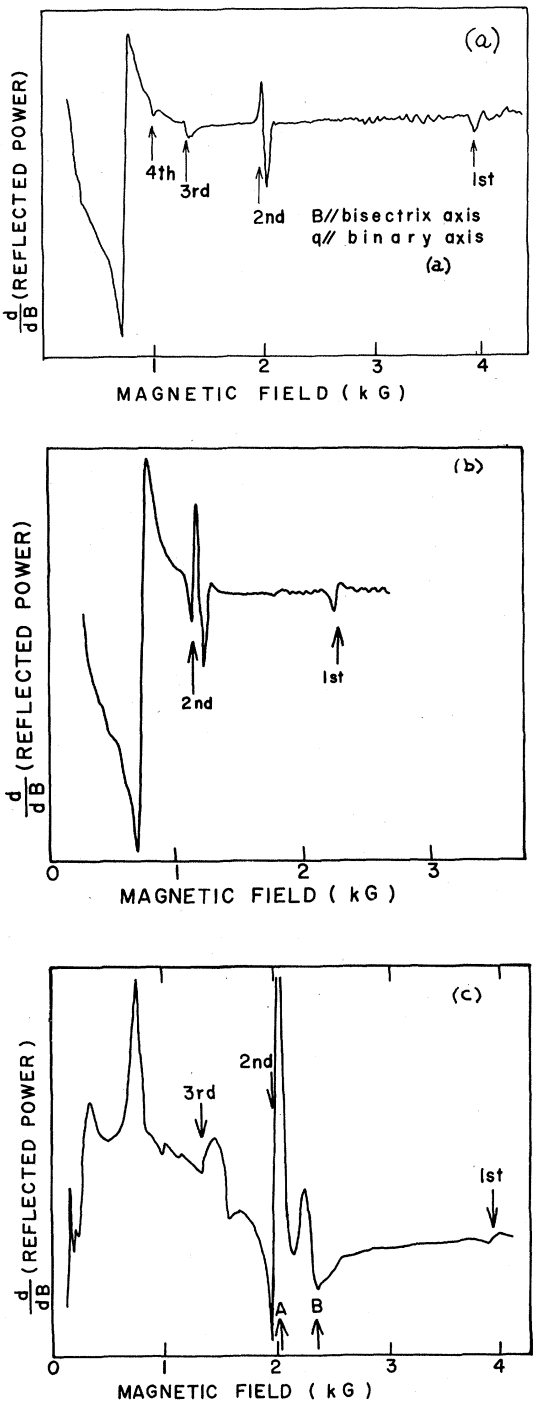

FIG. 4. Microwave reflection from a wedge-shaped bismuth single crystal as a function of magnetic field (derivative curve). Numbered arrows indicate the hole cyclotron harmonics. (a) $\vec{q} \parallel$ binary, $\vec{B} \parallel$ bisectrix axis; $f = 52.0$ GHz; $T = 1.6$ °K. (b) $\vec{q} \parallel$ binary axis, and the magnetic field is in a plane determined by the bisectrix and trigonal axes. The angle between the bisectrix axis and magnetic field is 27°; $f = 52.0$ GHz; $T = 1.6$ °K. (c) $\vec{q} \parallel$ trigonal, $\vec{B} \parallel$ bisectrix, $\vec{E}_{rf} \parallel$ binary axis; $f = 52.5$ GHz; $T = 1.6$ °K. The arrows A and B correspond to the arrows A and B in Figs. 1 and 8.

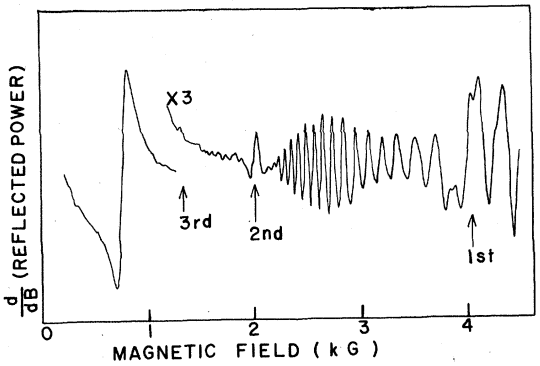

FIG. 5. Microwave reflection from a bismuth single crystal as a function of magnetic field (derivative curve). In this figure $\vec{q} \parallel$ binary, $\vec{E}_{rf} \parallel \vec{B} \parallel$ bisectrix axis; $f = 52.5$ GHz; $d = 0.411 \pm 0.002$ mm.

tions and Alfvén waves in the local regime. The coupling of transverse excitation with Alfvén waves can not be observed, since in this case qR is much less than one.

If the specimen is thick and wedge shaped, the Fabry-Perot interference pattern disappears and only the change of the surface impedance was observed as shown in Fig. 4(a). We can observe a weak peak near the fundamental resonance and a dielectric anomaly on the low-field side in addition to the cyclotron harmonics already seen in Fig. 2. As the static magnetic field is rotated from the bisectrix to the trigonal axis, the resonance line shape near the second harmonic becomes complex with a satellite peak on the low-field side as shown in Fig. 4(b). This peak corresponds to a transverse resonance (Fig. 1) which becomes stronger with increasing qR. Due to the characteristic mass anisotropy of bismuth, qR at the second harmonic becomes larger as the magnetic field is rotated from the bisectrix to the trigonal axis. Figure 4(c) shows the line shape in the vicinity of the second harmonic for the configuration $\vec{q} \parallel$ trigonal, $\vec{B} \parallel$ bisectrix, and $\vec{E}_{rf} \parallel$ binary axis. Since in this configuration qR at the resonance is still larger than that in Fig. 4(b), the peaks due to transverse and longitudinal resonance separate further as shown by arrows.

For the ordinary mode where $\vec{E}_{rf}$ is parallel to the magnetic field, the fundamental cyclotron resonance is stronger than the second harmonic as shown in Fig. 5. In this direction, the crystal symmetry is poor, and the extraordinary mode is not totally excluded. Consequently, the oscillatory variation of the reflected power due to the Alfvén wave interference is observed in this orientation as well.

IV. CALCULATION OF LINE SHAPE

In this section we shall calculate the line shape of the reflected power in terms of surface imped-

ance and compare the calculated line shapes with the experimental results presented in Sec. III. Hebel[6] has discussed the microwave absorption due to a slightly anomalous skin effect by calculating the surface conductivity for the weakly nonlocal case. His method is applicable both for diffuse and specular reflection, but unfortunately it is limited to the extremely weak nonlocal case where $R \ll$ skin depth or $qR \ll 1$. Therefore, we have employed the standard method of calculating the surface impedance, which has been extensively used in metals.[4,15–17]

We shall consider a semi-infinite sample in the yz plane of a Cartesian coordinate system. The wave vector is normal to the surface ($\vec{q} \parallel \hat{X}$) and the static magnetic field is parallel to the z axis. If the electrons are assumed to reflect specularly at the surface, the surface impedance is given by

$$Z = \frac{8i\omega}{c^2} \int_0^\infty \frac{dq}{q^2 - (\omega/c)^2 \epsilon^*} , \qquad (13)$$

where

$$\epsilon^* = \epsilon_{zz}$$

for the ordinary mode, and

$$\epsilon^* = (\epsilon_{xx}\epsilon_{yy} + \epsilon_{xy}^2)/\epsilon_{xx}$$

for the extraordinary mode. In the case of metals the density of carriers is so high that $qR \gg 1$ and the dielectric functions can be expanded asymptotically in powers of $1/qR$. In this limit the integrand of the expression (13) has no pole in the region of small wave number, and can be analytically integrated as was done by Azbel'-Kaner and other authors.[15–17] For bismuth, however, the carriers are compensated and their densities are so low that the integrand has poles in the region of low wave number. In Fig. 6 the results of the calculation[23,24] for the second harmonic are compared with the experiment in the configuration $\vec{q} \parallel$ binary, $\vec{B} \parallel$ bisectrix, and $\vec{E}_{rf} \parallel$ trigonal axis. In this calculation only the lowest-order term (X^2) was taken into account and the results depend negligibly upon the upper limit of integration. For the third harmonic shown in Fig. 7 the convergence is very poor and is quite sensitive to higher-order terms, since qR is about unity around the third harmonic. Therefore, for the integration from 0 to 4, the in-

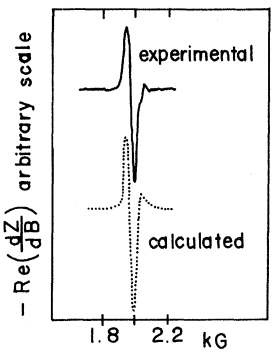

FIG. 6. Real part of the derivative of the surface impedance as a function of magnetic field. The solid line represents the experimental curve for the microwave reflection in the vicinity of the second harmonic of the hole cyclotron resonance. The dotted line is the calculated line shape, assuming $\omega\tau = 100$ and retaining terms up to the order of $(qR)^2$.

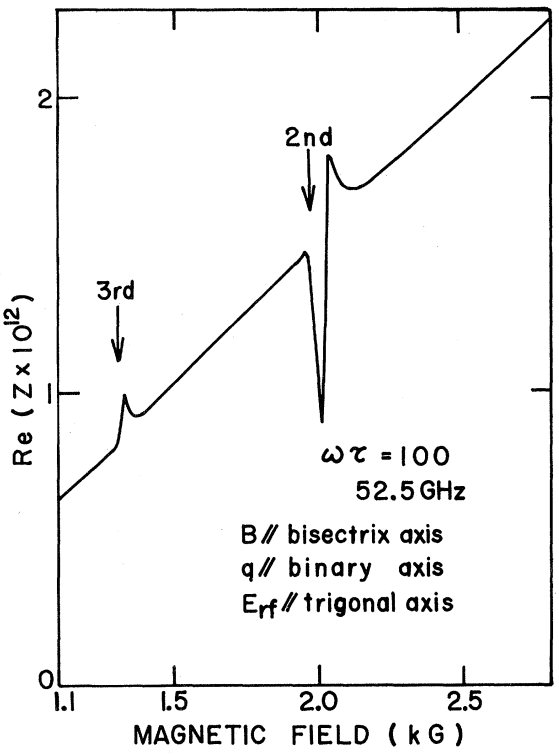

FIG. 7. Real part of surface impedance (calculated) as a function of magnetic field when $\vec{q} \parallel$ binary, $\vec{B} \parallel$ bisectrix, $\vec{E}_{rf} \parallel$ trigonal axis; $f = 52.5$ GHz; and $\omega\tau = 100$.

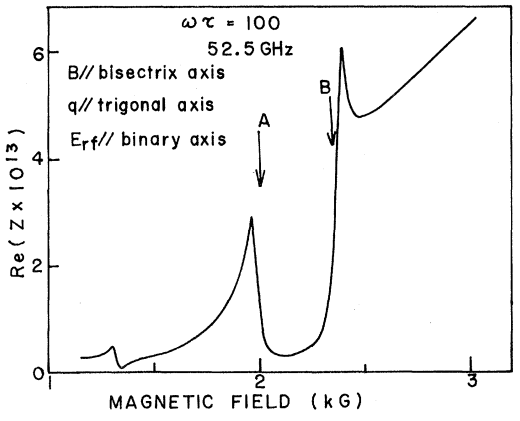

FIG. 8. Real part of the surface impedance (calculated) as a function of magnetic field for $\vec{q} \parallel$ trigonal, $\vec{B} \parallel$ bisectrix, $\vec{E}_{rf} \parallel$ binary axis; $f = 52.5$ GHz; and $\omega\tau = 100$. The arrows A and B correspond to the arrows in Fig. 7, respectively, and to A and B in Fig. 1.

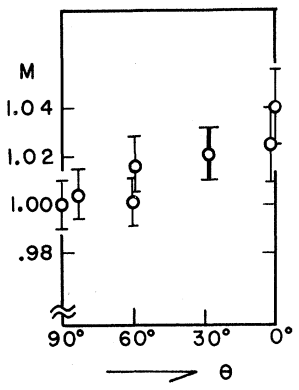

FIG. 9. Shift of anomalies with angle $\theta°$ between $\vec{E}_{rf}$ and $\vec{B}$ ($\vec{q}\parallel$ binary, $\vec{B}\parallel$ bisectrix axis). Ordinate M is $H_2(\theta)/H_2(90°)$, where $H_2(\theta)$ is the middle point of the anomaly near the second harmonic measured relative to the anomaly in the extraordinary configuration.

tegrand was expanded up to X^{20}, and for that from 4 to infinity, the asymptotic form was employed. The result reproduces the experimental curve fairly well.

When $\vec{q}\parallel$ trigonal, $\vec{B}\parallel$ bisectrix, and $\vec{E}_{rf}\parallel$ binary axis, qR is nearly equal to unity in the neighborhood of the second harmonic due to the anisotropy of the hole mass. In this case the transverse and the longitudinal excitations are clearly separated. The result of the calculation for surface impedance is shown in Fig. 8, which should be compared with the observed derivative curve shown in Fig. 4(c). The arrows in Figs. 4(c) and 8 are the transverse and longitudinal resonances, respectively (points A and B in Fig. 1). The field intervals delineated by arrows on the experimental and calculated curves agree very well [see Figs. 4(c) and 8]. However, the experimental relative intensities of these two peaks are reversed from the calculated values. Although the peak for the transverse resonance is stronger in the experiment, the high-field edge (B) of the absorption curve is steeper than the low-field edge (A) in the calculation. This discrepancy probably results both from the failure of the assumption that the carriers reflect specularly at the surface and the neglect of off-diagonal elements, arising from the tilting effect of electron Fermi surfaces of the dielectric tensor.

If we attribute the series of anomalies in the reflection curve to the harmonics of the Azbel'-Kaner cyclotron resonance, we obtain the value $(0.213 \pm 0.002)m_0$ as the cyclotron mass of holes for $\vec{B}\parallel$ bisectrix axis. However, according to the above discussion, we must analyze the line shape including the shifts of peaks from the positions of the exact cyclotron harmonics. The mass value determined in this manner is $(0.210 \pm 0.002)m_0$. The difference between these two masses is greater than one standard deviation.

When the polarization of the microwaves is rotated from the extraordinary to ordinary configuration, the center of the anomaly at the second harmonic shifts to the higher-field side as shown in Fig. 9. Since the transverse resonance which is dominant for the ordinary configuration is located on the lower-field side compared with the position of the longitudinal resonance which is dominant for the extraordinary configuration, the line would shift to the low-field side with rotation of the microwave polarization from perpendicular to parallel to the magnetic field if the cyclotron mass were constant. So we have concluded that the limiting-point mass which is responsible for the resonance in the ordinary configuration is larger than the mass of the extremum orbit.[4] From these data the limiting-point mass is estimated to be $(0.217 \pm 0.003)m_0$.

ACKNOWLEDGMENTS

The authors would like to express their sincere thanks to Professor Y. Uemura and X. Akabane for very stimulating discussions. We are much obliged to Dr. S. Nagata for collaboration at the early stages of the experiment. The kind help and discussion by Dr. S. Takano throughout the work is highly appreciated. The authors would like to express their gratitude for the grant by the Toyo Rayon Science Foundation.

[1]M. S. Khaikin, R. T. Mina, and V. S. Edel'man, Zh. Eksperim. i Teor. Fiz. 43, 2069 (1962) [Sov. Phys. JETP 16, 1459 (1962)].

[2]G. E. Smith, L. C. Hebel, and S. J. Buchsbaum, Phys. Rev. 129, 154 (1963).

[3]Yi-Han Kao, Phys. Rev. 129, 1122 (1963).

[4]V. S. Edel'man and M. S. Khaikin, Zh. Eksperim. i Teor. Fiz. 49, 107 (1965) [Sov. Phys. JETP 22, 107 (1965)].

[5]L. C. Hebel, E. I. Blount, and G. E. Smith, Phys. Rev. 138, A1636 (1965).

[6]L. C. Hebel, Phys. Rev. 138, A1641 (1965).

[7]G. A. Williams, Phys. Rev. 139, A771 (1965).

[8]H. T. Isaacson and G. A. Williams, Phys. Rev. 177, 738 (1969).

[9]R. T. Isaacson and G. A. Williams, Phys. Rev. 185, 682 (1969).

[10]S. Nagata and H. Kawamura, J. Phys. Soc. Japan 24, 480 (1968).

[11]S. Takano and H. Kawamura, J. Phys. Soc. Japan 28, 349 (1970).

[12]G. E. Everett, Phys. Rev. 128, 2564 (1962).

[13]R. C. Chambers, Proc. Phys. Soc. (London) 86, 305 (1965).

[14]T. W. Moore, Phys. Rev. 165, 864 (1968).

[15]M. Ya. Azbel' and E. A. Kaner, J. Phys. Chem. Solids 6, 113 (1958); Zh. Eksperim. i Teor. Fiz. 30, 811 (1956) [Sov. Phys. JETP 3, 772 (1956)].

[16]S. Rodriquez, Phys. Rev. 112, 1616 (1958).

[17]D. C. Mattis and G. Dresselhaus, Phys. Rev. 111, 403 (1958).

[18]J. J. Quinn and S. Rodriguez, Phys. Rev. 128, 2487 (1962).

[19]At the immediate vicinity of the cyclotron harmonics, the "high-frequency wave" can penetrate in the nonlocal regime as shown by P. M. Platzman, W. M. Walsh, Jr.,

and E-Ni Foo, Phys. Rev. 172, 689 (1969).
[20]P. W. Anderson, Phys. Rev. 100, 749 (1955).
[21]I. B. Bernstein, Phys. Rev. 109, 10 (1958).
[22]C. K. N. Patel and R. F. Slusher, Phys. Rev. Letters 21, 1593 (1968).
[23]Band parameters employed in the calculation are as follows: $m_1=0.0011$, $m_2=1.70$, $m_3=0.0301$, $m_4=0.177$, $M_1=0.700$, $M_3=0.063$, carrier density $=2.9\times10^{17}$ cm^{-3}, and Fermi energy of holes $=11.45$ meV.
[24]The calculations were carried out using an NEAC 2200 at Computer Center of Osaka University.

PHYSICAL REVIEW B VOLUME 3, NUMBER 10 15 MAY 1971

Phenomenological Molecular-Field Theory of the Mott-Wigner Transition in Magnetite

J. B. Sokoloff
Northeastern University, Boston, Massachusetts 02115
(Received 13 July 1970; revised manuscript received 17 August 1970)

The measurement by Verwey and Haayman of the variation of the transition temperature of magnetite with stoichiometry is discussed in terms of the molecular-field solution of a lattice-gas model of the Mott-Wigner insulator-to-metal transition. This model gives rise to a second-order phase transition. The observed first-order transition is reproduced by substituting a phenomenologically screened interaction, in which the dielectric constant causing the screening decreases with increasing order parameter. Since the phenomenological screening necessary to produce the observed results is very large compared to that expected on the basis of electronic screening, we postulate that the dielectric constant includes the effect of local charge polarization accompanying the ordering. It is possible to obtain a consistent picture of many of the experimental data on magnetite using this model. Inelastic neutron scattering and optical absorption are discussed as means of observing the elementary excitations of the system and to deduce some of the parameters in the theory. The low-lying excitations in the ordered (i.e., insulating) state are shown to be excitons with flat dispersion (i.e., their energies do not depend on wave vector); their energies and cross sections are calculated.

I. INTRODUCTION

It was suggested by Mott[1,2] that the insulating state of magnetite could be described by a Wigner electron lattice,[3] and the insulator-to-metal transition as a melting of this lattice. Objection was raised to this picture by Rosencwaig[4] because it predicted an increase in the transition temperature as the number of electrons in the system is decreased, instead of the decrease that is actually observed.[5] In Secs. II and III, the insulator-to-metal transition in magnetite is described using a lattice-gas model, which is similar to the molecular-field solution of the Ising model of antiferromagnetism. The model is found to agree qualitatively with the results of Verwey and Haayman on the variation of transition temperature with stoichiometry. The introduction of a phenomenological interaction which varies rapidly with the number of free carriers in the system (and hence with the order parameter) makes it possible to reproduce the observed first-order transition. The behavior of the specific heat and conductivity near the transition temperature is discussed in terms of this effective-interaction version of the lattice-gas model. In Sec. IV, the elementary excitation spectrum, as well as the inelastic-neutron-scattering and infrared-optical-absorption cross sections, is found. The low-lying excitations are found to be excitons with flat wave-vector-independent bands, and their energy spectrum is calculated. Measurement of the exciton energies would make it possible to deduce some of the parameters in the theory of Secs. II and III.

This model is similar to a model introduced by Cullen and Callen[6] to describe magnetite in that both models introduce a temperature-dependent order parameter to describe the phase transition. Cullen and Callen's model is a Hartree-Fock-approximation energy-band model. The present model leaves out all discussion of details of the electronic energy states, since it is not known as yet whether band theory or small-polaron hopping is a better description of magnetite. The band theoretic description of the problem of Ref. 6 is introduced in Sec. III, however, to describe the pressure dependence of the transition temperature. The treatment presented here shows how the dependence of transition temperature on stoichiometry can be explained using an electron-lattice model. With the phenomenological interaction introduced later, the model is shown to allow a simple and consistent interpretation of much of the experimental data on magnetite using a few simple param-